

Hybrid Graphene-Gold Nanoparticle-Based Nucleic Acid Conjugates for Cancer-Specific Multimodal Imaging and Combined Therapeutics

Letao Yang, Tae-Hyung Kim, Hyeon-Yeol Cho, Jeffrey Luo, Jong-Min Lee, Sy-Tsong Dean Chueng, Yannan Hou, Perry To-Tien Yin, Jiyoun Han, Jong Hoon Kim, Bong Geun Chung, Jeong-Woo Choi, and Ki-Bum Lee*

Nanoparticle-based nucleic acid conjugates (NP-NACs) hold great promise for theragnostic applications. However, several limitations have hindered the realization of their full potential in the clinical treatment of cancer and other diseases. In diagnoses, NP-NACs suffer from low signal-to-noise ratios, while the efficiency of NP-NACs-mediated cancer therapies has been limited by the adaptation of alternative prosurvival pathways in cancer cells. The recent emergence of personalized and precision medicine has outlined the importance of having both accurate diagnosis and efficient therapeutics in a single platform. As such, the controlled assembly of hybrid graphene oxide/gold nanoparticle (Au@GO NP)-based cancer-specific NACs (Au@GO NP-NACs) for multimodal imaging and combined therapeutics is reported. The developed Au@GO NP-NACs show excellent surface-enhanced Raman scattering (SERS)-mediated live-cell cancer detection and multimodal synergistic cancer therapy through the use of photothermal, genetic, and chemotherapeutic strategies. Synergistic and selective killing of cancer cells are then demonstrated using *in vitro* microfluidic models. Moreover, with the distinctive advantages of the Au@GO NP-NACs for cancer theragnostics, precision cancer treatment through the detection of cancer cells *in vivo* using SERS followed by efficient ablation of tumors is shown. Therefore, the Au@GO NP-NACs can pave a new road for advanced disease theragnostics.

tumor microenvironment (TME) as well as a multitude of genetic/epigenetic alterations leading to abnormal cell behaviors.^[1,2] Conventional cancer therapeutic approaches have shown limited success against various cancers due to the heterogeneity of the TME and complex oncogenic signaling pathways in cancer.^[1,3] Regarding the current challenges and opportunities in cancer research, nanotheragnostics have been demonstrated as an advanced approach for early cancer diagnosis, accurate cancer prognosis, and effective cancer treatment.^[4,5,6] Typically, these nanotheragnostic systems are multifunctional nanosystems that can integrate cancer-specificity, imaging, and treatment modalities into nanomaterials for effectively combined cancer therapeutics.^[7] For example, the recent development of nanomaterial-based nucleic acid conjugates (NACs) has shown excellent potential as an innovative theragnostic tool for advanced cancer research.^[8,9,10] Given that the primary goal of personalized medicine is to target the disease-specific genetic information of patients, NACs have a


clear advantage by having the ability to sense endogenous biomarkers.^[11,12] However, remaining issues include enzymatic degradation and inefficient cellular uptake of NAC therapeutics, which need to be addressed before the full realization of

1. Introduction

Cancer is considered one of the most complex and aggressive diseases that is dynamically controlled by the complexity of the

Dr. L. Yang, Dr. T.-H. Kim, Dr. H.-Y. Cho, J. Luo, Dr. S.-T. D. Chueng, Y. Hou, Dr. P. T.-T. Yin, Prof. K.-B. Lee
Department of Chemistry and Chemical Biology
Rutgers
The State University of New Jersey
123 Bevier Road, Piscataway, NJ 08854, USA
E-mail: kblee@rutgers.edu

Dr. H.-Y. Cho, Prof. J.-W. Choi
Department of Chemical and Biomolecular Engineering
Sogang University
35 Baekbeom-ro, Mapo-gu, Seoul 04107, Republic of Korea

 The ORCID identification number(s) for the author(s) of this article can be found under <https://doi.org/10.1002/adfm.202006918>.

Dr. J.-M. Lee, Prof. B. G. Chung
Department of Mechanical Engineering
Sogang University
35 Baekbeom-ro, Mapo-gu, Seoul 04107, Republic of Korea

Dr. J. Han, Prof. J. H. Kim
College of Life Sciences and Biotechnology
Science Campus
Korea University
145 Anam-ro, Seongbuk-gu, Seoul 02741, Republic of Korea

DOI: 10.1002/adfm.202006918

NAC-based cancer therapeutics is achieved.^[8,13,14] The integration of NACs into multifunctional nanomaterials can overcome the above hurdles.

Among various nanomaterials for constructing nanomaterial-NACs, carbon- (e.g., graphene and carbon nanotube) and noble metal (e.g., gold)-based plasmonic nanomaterials have shown promising results for cancer applications due to their unique physicochemical properties at the nanoscale.^[15–17] Graphene oxide (GO) and its derivatives, with amphiphilic surfaces and high surface areas, have been proven as excellent multifunctional delivery platforms for small molecule drugs and nucleic acids.^[12,18,19] Moreover, efficient binding of single-stranded oligonucleotides onto GO surfaces and their reversible detachment in the presence of complementary DNA/mRNA have enabled selective and sensitive detection of crucial oncogenes in live cancer cells.^[19] Meanwhile, plasmonic nanomaterials have been widely utilized for constructing ultrasensitive biosensors as well as developing advanced phototherapies, owing to their unique ability to amplify optical fields nonlinearly through localized surface plasmonic resonance (LSPR).^[16,20] Furthermore, some recent studies have reported synergistic therapeutic results between the two (carbon-based and plasmonic) groups of nanomaterials for a variety of biomedical applications.^[10,21,22] We hypothesized that the combination of unique biological properties from NACs with the excellent physicochemical properties of hybrid graphene oxide (GO)/plasmonic gold (Au) nanoparticles would enable scientists to develop advanced cancer-specific multimodal imaging and combined therapeutics. This task necessitates the innovative design and synthesis of hybrid plasmonic-graphene nanomaterial-based NACs for in vitro and in vivo nanotheragnostic applications.

Herein, we describe a novel strategy for the design, synthesis, and application of multifunctional hybrid graphene oxide/plasmonic gold-based nucleic acid conjugates (**Au@GO NP-NACs**) to advance precision cancer medicine. Remarkably, we demonstrate the controlled assembly of different graphene/gold hybrid nanostructures and identified Au@GO NPs as an ideal platform for constructing the theragnostic NACs. As a proof-of-concept, we demonstrated its potential applications for overcoming critical hurdles in precision cancer therapy, such as the identification of effective multimodal therapeutics, site-specific drug/gene delivery, and noninvasive imaging (Figure 1a). Although some demonstrations on cancer-specific multimodal imaging has been previously reported, the development of nondestructive approaches with improved resolutions that can be potentially combined with or replace current clinical standard [e.g., magnetic resonance imaging (MRI)] is still an urgent need.^[5] Similarly, while both noble metal nanoparticle and graphene-based combined cancer therapeutics have been developed, the simultaneous incorporation of advanced multimodal imaging and delivery of multiple clinically relevant chemo/gene therapeutics could maximize their potential in cancer treatment and facilitate their clinical translation.^[17] For this purpose, our Au@GO NP-NACs are designed to have i) a core-shell structure with high colloidal stability and efficient cellular uptake; ii) excellent dark-field cell imaging (DFI) modality; iii) a distinctive surface-enhanced Raman spectroscopy (SERS) properties for probing oncogenes in a nondestructive manner,

and iv) a dual cancer therapeutic platform [photothermal (PT) and chemotherapies] (Figure 1b). Further, cancer imaging and detection are achieved by conjugating Raman dye (Cy5)-labeled nucleic acid (e.g., AntiSense OligoNucleotide (**ASON**)) that specifically targets oncogenes (BCL2) onto Au@GO NPs via π - π stacking (Au@GO NP-BCL2-NAC for short). While our system is highly modular and a variety of different oncogenes can be targeted, we focused on BCL2 as a proof-of-concept, as the upregulated pro-survival BCL2 gene has been identified as a cancer hallmark and proven to be a suitable target for cancer diagnosis.

To further validate our cancer nanotheragnostic platform based on Au@GO NP-NAC, we then demonstrated the accurate detection of tumor markers followed by the effective suppression of tumor growth, which could address the critical issue of tumor heterogeneity. Using Au@GO NP-BCL2-NAC, we can successfully differentiate cancer cells from control cells using SERS (Figure 1b). More specifically, the delivery of an Au@GO NP-BCL2-NAC conjugated with Cy5 Raman dye (Au@GO NP-Cy5-BCL2-NAC) into cancer cells resulted in selective binding between the ASONs and the over-expressed BCL2 mRNAs, leading to the disruption of π - π stacking via duplex formation and the subsequent release of Raman dye (Cy5) molecules as indicated by the reduced SERS signal (Figure 1b). Meanwhile, the targeted oncogene (*BCL2*) expression was reduced simultaneously. By combining the delivery of clinically approved anti-cancer drugs (e.g., doxorubicin), repression of the drug-resistance gene (*BCL2*) expression through antisense ASON, and phototherapies in a single platform, a near-complete removal of cancer cells was achieved in vitro and in vivo (Figure 1c). Finally and importantly, the general applications of our therapeutic platform were testified a comprehensive multicancer cell line (9 different lines with distinctive cancer origins) assay. In this way, we successfully established an Au@GO NP-NAC-based platform that can provide distinctive cancer detection modalities and effective combinatorial therapies to advance cancer theragnostics.

2. Results and Discussions

2.1. Design and Synthesis of Hybrid Graphene Oxide/Gold Nanoparticles (Au@GO NPs) for the Specific and Efficient Delivery of Therapeutic Modalities into Cancer Cells

Plasmonic metal-graphene hybrid nanomaterials have shown a wide spectrum of attractive properties for cancer theragnostics, but colloidal instability or bulkiness limits their practical use.^[23,24] Also, the physical and biological properties of plasmonic metal-graphene hybrid nanomaterials are highly sensitive to their hybrid structures, requiring a versatile method for precisely controlling the assembly between metal nanoparticles and GO.^[17] To this end, we first established a unique generalized electrostatic self-assembly method to controllably create different plasmonic metal-GO hybrid nanomaterials, which include 0D core-shell structured GO-encapsulated gold nanoparticles (Au@GO NPs, experimental condition), 0D reduced GO-encapsulated gold nanoparticles (Au@rGO NPs), 1D GO-encapsulated gold nanorods (Au@GO NRs), as well

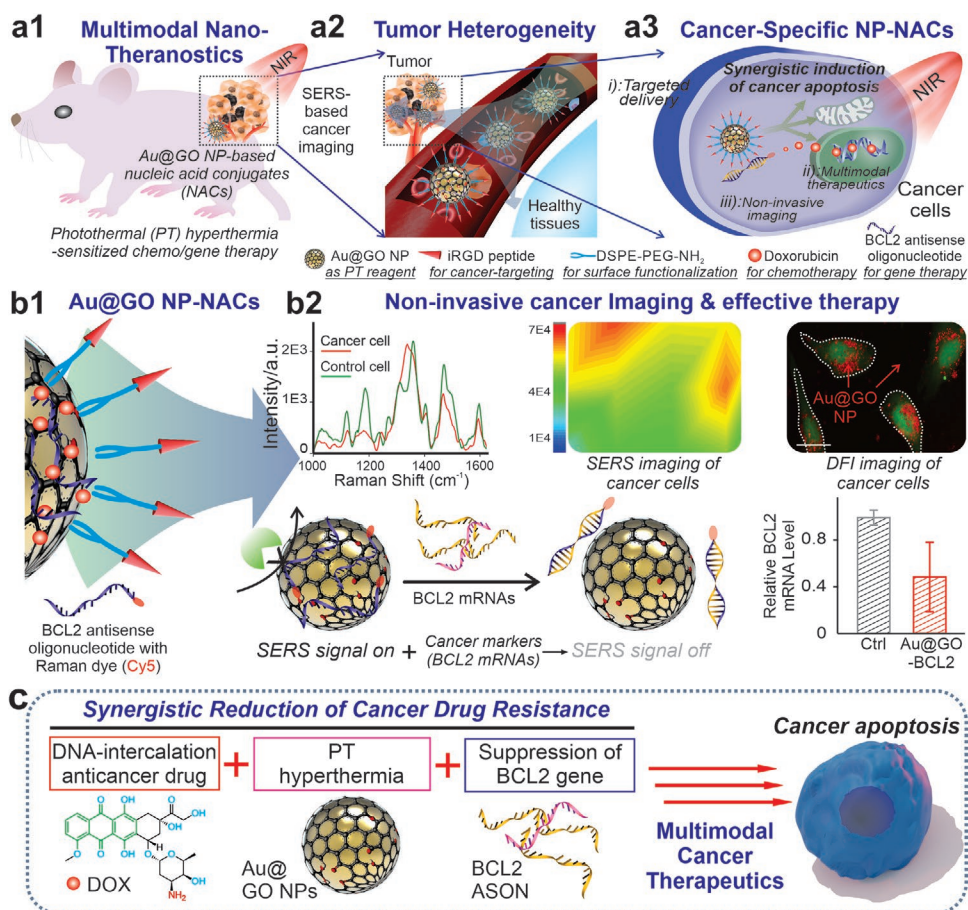


Figure 1. Schematic diagram illustrating the hybrid graphene oxide/gold nanoparticles-nucleic acid conjugates (Au@GO NP-NACs) for cancer cell imaging and multimodal therapeutics. a) Schematic diagrams showing the working principles of Au@GO NP-NAC-based multimodal cancer nanotheragnostics. By constructing an Au@GO NP-NAC-based multifunctional platform that provides photothermal hyperthermia-enhanced chemo/gene therapy, tumor heterogeneity could be targeted effectively for a strong suppression of cancer cell growth in vitro and in vivo through combined cancer therapeutics. b) Schematic diagram of the Au@GO NP-NAC-mediated cancer cell imaging, which includes SERS imaging and dark-field imaging (top row) and gene therapy that targets a cancer pro-survival gene responsible for drug resistance (bottom row). In the top row, Raman dye-functionalized antisense oligonucleotide (ASON) loaded on Au@GO NP demonstrates SERS due to the localized surface plasmon resonance (LSPR) from Au NP core, the detection of genes based on the selective detachment of ASON in the presence of complementary RNA for surface-enhanced Raman scattering (SERS)-based imaging, and the simultaneous silencing of a drug resistance (BCL2) gene in cancer cells (shown in the bottom row). Scale bar in the DF1 imaging on the right: 100 μm . $*P < 0.05$ by student's *t* test. $n = 3$ independent experiments. c) Proposed mechanisms on the synergistic multimodal cancer theragnostics based on the Au@GO NP-ASON therapeutic platform, which is mediated through collective activation of intracellular proapoptotic pathways and suppression of antiapoptotic pathways.

as 2D gold nanoparticle-decorated GO (Au NP-GO assembly) (Figure 2a,b; and Figures S1 and S2, Supporting Information). Specifically, the core-shell hybrid nanostructures were synthesized by the slow addition of positively charged, diluted solution ($<100 \mu\text{g mL}^{-1}$) of gold nanoparticles (+33 mV, ≈ 40 nm, for Au@GO NP and Au@rGO NP) or gold nanorods (+11 mV, 10 nm width and 40 nm length, for Au@GO NR) into concentrated solutions ($>3.0 \text{ mg mL}^{-1}$) negatively charged GO (-54 mV, 110 nm) with (for Au@rGO NP) or without (for Au@GO NP) reduction by ascorbic acid (Figure 2a; and Figures S1 and S2, Supporting Information). Meanwhile, the Au NP-GO assembly is synthesized by simply reversing the order of reaction by adding diluted GO solution into a concentrated solution of Au NPs (Figure 2a). All these structures show excellent enhancement effect on the electromagnetic field, according to our finite-difference time-domain (FDTD) simulation, which is

desired for our following applications in cancer imaging and PT therapies (Figure 2a; and Figure S2, Supporting Information). However, although rGO, Au NR, and Au NP assemblies have been reported to show stronger photothermal properties than GO and Au NP alone, we found that the Au@rGO NPs and Au NP-GO assembly show poor colloidal stability, likely due to their hydrophobic surfaces and bulkiness, respectively (Figure 2c; and Figure S3, Supporting Information). Au@GO NRs showed improved colloidal stability, but they were slightly cytotoxic at higher concentrations ($100 \mu\text{g mL}^{-1}$), which could originate from the cetyltrimethylammonium bromide (CTAB) ligands based on previous literature (Figure 2d).^[25] Considering that our following applications would require several steps of surface modifications, and a mild photothermal effect is sufficient for our purpose of sensitizing cancer cells, we focused on the Au@GO NPs that have excellent colloidal stability,

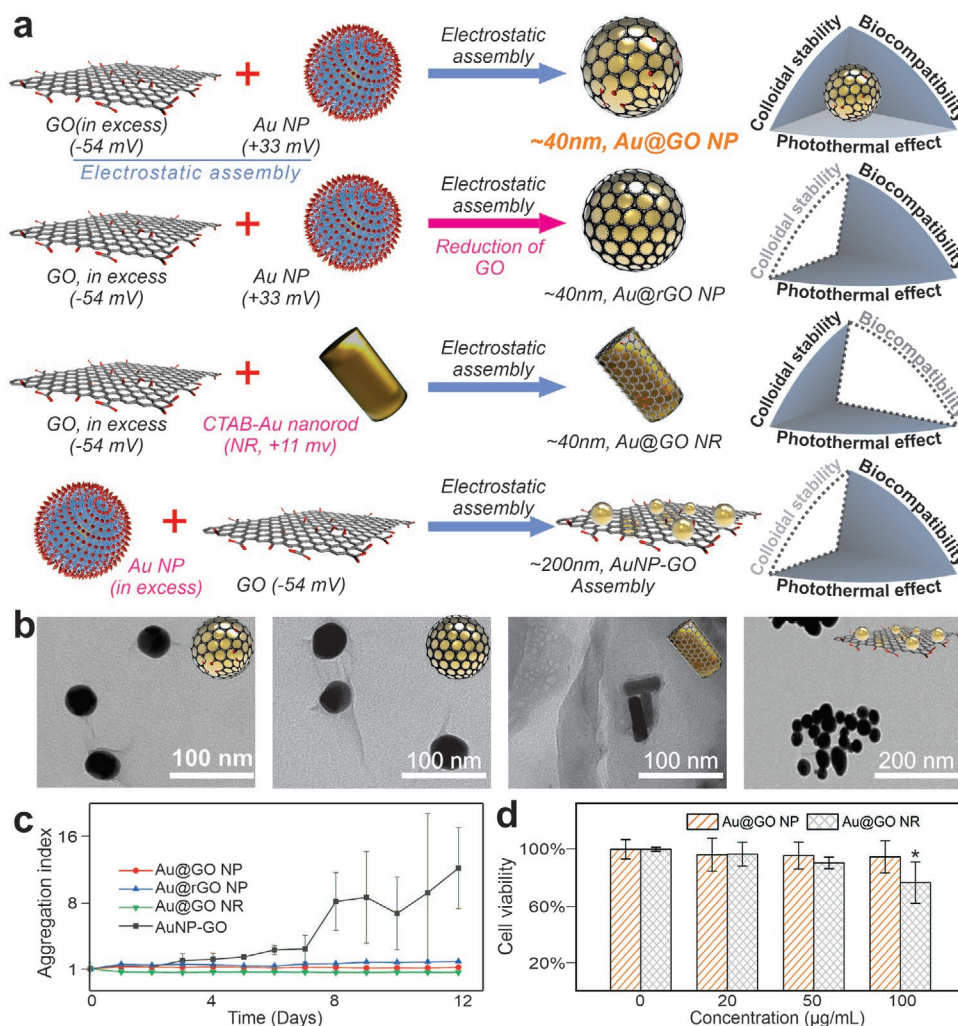


Figure 2. Controlled synthesis of gold-graphene hybrid nanomaterials. a) Schematic diagrams showing the controlled synthesis of varying gold-graphene hybrid nanomaterials with distinct colloidal stability, biocompatibility, and capability of inducing photothermal hyperthermia. NP represents nanoparticles, RGO represents reduced graphene oxide, and NR represents nanorods. b) Representative transmission electron microscope (TEM) images showing the successfully synthesized graphene/gold hybrid nanoparticles. c) Higher colloidal stability of Au@GO NP and AuNR@GO compared to the Au@rGO NP based on a graph comparing the aggregation index of different structures of graphene/gold nanoparticles. d) A better biocompatibility of Au@GO NP compared to Au@GO NR based on a MTS assay and using cancer and fibroblast cell lines. The CTAB ligands in the Au NRs may contribute cytotoxicity of Au@GO NR. * $P < 0.05$, by student's t test. $n = 3$ independent experiments.

biocompatibility, as well as a proper size range for cellular uptake for the current study.^[17,23]

Moreover, we hypothesized that our synthesized Au@GO NP could incorporate high-contrast imaging of cancer cells via a robust plasmonic effect and achieve high cellular uptake efficiency by having a proper size and shape range for endocytosis (Figure 3a). We confirmed our hypothesis by first investigating the plasmonic effect using FDTD simulation, which shows a clearly enhanced light field intensities in the proximity of Au NPs (Figure 3b). The GO encapsulating the Au NP could readily absorb the enhanced light, which is evidenced by the over threefold higher absorption at the NIR range of light in the UV-vis spectrum of Au@GO NP as compared to Au NP or GO alone (Figure 3c). As a result, we observed exponentially increased D and G band peak intensities of GO in the Raman spectra of Au@GO NP compared to GO alone, an effect

known as SERS, which is desired for our cancer biosensing and imaging applications (Figure 3d).^[10] Additionally, a high contrast DFI modality was also enabled by the plasmonic core in the Au@GO NP (Figure 3e). Although many fluorescence-based-cancer imaging methods have been widely applied for nanoparticle-based drug delivery systems, graphene and GO can quench the fluorescence of conjugated dyes via Förster resonance energy transfer (FRET), leading to poor quality of fluorescence imaging.^[26,27] In this regard, Au@GO NP could address this challenge as both DFI and SERS signals are typically sharp and not affected by GO. Utilizing the DFI and SERS, we successfully confirmed the high delivery efficiency of Au@GO NP into cancer cells that is crucial for our therapeutic platform (DFI, Figure 3e). Specifically, cancer cells that uptake Au@GO NPs show extremely high contrast and low noise levels, further supporting Au@GO NP as an excellent

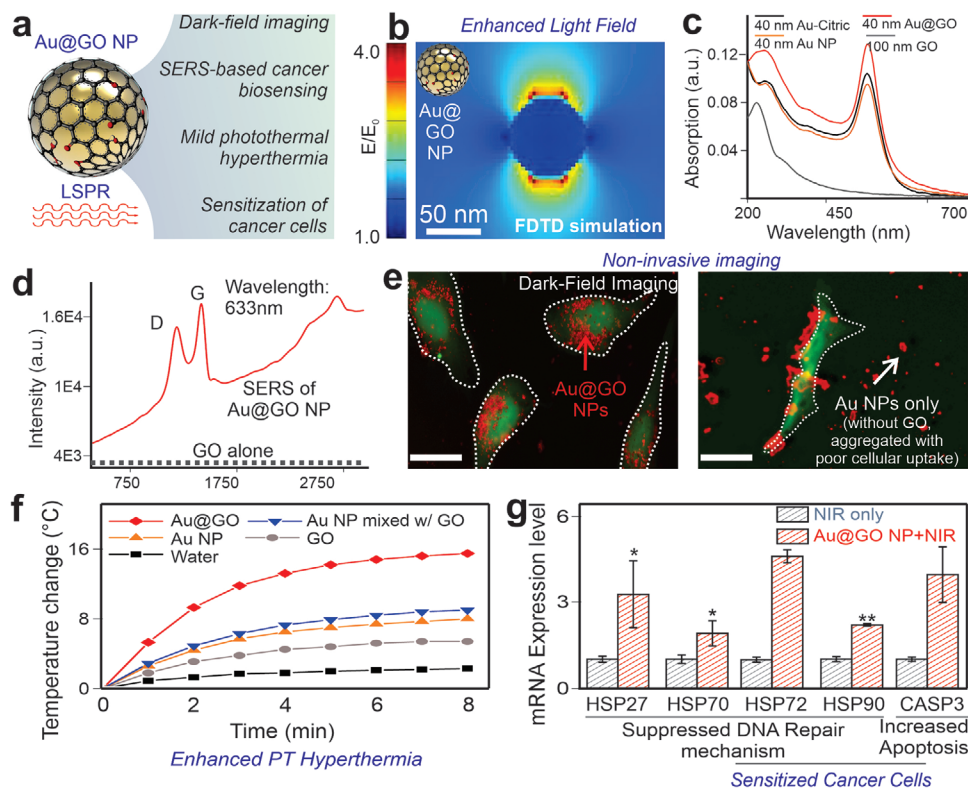


Figure 3. Au@GO NP-based high-contrast cancer cell imaging and mild photothermal hyperthermia for sensitization of cancer cells. a) A schematic diagram showing the imaging modalities and photothermal sensitization of cancer cells enabled by the plasmonic effect of the Au NP core. Synthesis of Au@GO NP via the controlled electrostatic assembly. b) FDTD simulation on the electromagnetic field enhancement nearby the surface of a 40 nm sized gold nanoparticle. This simulation further explains LSPR-enhanced light matter interactions and photothermal effects. c) UV-vis absorption spectroscopy showing enhanced absorption at NIR region in the Au@GO NP. d) Raman spectroscopy of GO and Au@GO NP showing the significantly enhanced D and G bands of GO for SERS biosensing. e) DFI imaging of a GFP labeled cell line using Au@GO NP (left) and cysteamine-functionalized gold nanoparticle (Au NP, image on the right). Scale bar: 100 μm . The red color was used as a pseudocolor for the DFI signals scattered from Au@GO NP. DFI from Au@GO NP can be observed intracellularly with high contrast while GO barely show signals. f) A photothermal assay using a low-density laser for irradiating the Au@GO NP aqueous solution as well as the control solutions. Only the Au@GO NP solution shows a distinctive temperature change, which suggests an enhanced photothermal effect. g) The activation of HSPs and Caspases by mild photothermal hyperthermia using a NIR laser to sensitize cancer cells toward apoptosis by activating HSP and Caspase pathways. * $P < 0.05$, ** $P < 0.01$ by student's t test. $n = 3$ independent experiments.

reagent for noninvasive cancer imaging in vitro, as DFI is compatible with live cell detection. As a control, cells cultured with GO alone did not yield any noticeable DFI signals, thereby supporting the LSPR origin of Au@GO NP-enhanced DFI (Figure 3e). Taken together, our Au@GO NPs exhibited excellent cellular uptake by cancer cells, high biocompatibility with somatic cells, and have distinctive imaging modalities, all of which are desired for cancer theragnostic applications.

2.2. Mild Photothermal Hyperthermia Induced by Au@GO NPs for Sensitizing Cancer Cells

Another critical criteria for constructing our cancer therapeutic platform is the capability of Au@GO NP to enhance PT hyperthermia, which has been proven as a robust strategy to improve the outcome of gene therapy and chemotherapy by activating the heat shock protein (HSP) pathway and sensitizing cancer cells toward a proapoptotic status in a spatiotemporally controlled manner.^[28–30] Specifically, our cancer

therapeutic approach is based on the delivery of BCL2 anti-sense oligonucleotide (BCL2-ASON) and a Topoisomerase II anticancer drug (doxorubicin) to synergize with the activation of HSP by mild hyperthermia for suppression of DNA repair mechanisms, as well as activating caspase pathways (Figure 1c). In this regard, we hypothesized that our core-shell Au@GO NP with GO adjacent to plasmonic nanoparticles could be advantageous for amplifying the local light field and enhancing photothermal effects, which has been supported by the FDTD simulation as well as UV-vis absorption spectrum experiments (Figure 3a–c).^[22] To directly validate our hypothesis on the enhanced PT hyperthermia from the Au@GO NP, we then performed additional characterization on the NIR laser-induced temperature increase from Au@GO NP compared to its two individual components (Au NP alone and GO alone) (Figure 3f). As shown in Figure 3f, at identical concentrations and low NIR laser intensity (1.2 W cm^{-2}), water alone resulted in a negligible temperature increase ($\Delta T < 2 \text{ }^\circ\text{C}$), suggesting minimal nonspecific heating from the laser. In contrast, the temperature of Au NP and GO solutions increased by 5 and

7 °C, respectively, which is consistent with literature reports as both Au NP and graphene nanomaterials are widely used photothermal reagents.^[17,22] However, the Au@GO NP solution showed the highest temperature increase of 15 °C. Therefore, we can conclude that a synergy exists between Au NP and GO for PT hyperthermia induction. Although only mild temperature increase is typically required to sensitize cancer cells, the increased PT effects in Au@GO NP can ensure a better tumor tissue penetration depth for in vivo applications. As such, we validated that Au@GO NP displays synergistically enhanced NIR PT hyperthermia for cancer therapeutic applications.

Next, we sought to investigate whether the Au@GO NP-based NIR PT hyperthermia could sensitize cancer cells by analyzing HSP and caspase gene expression through a quantitative reverse transcription-polymerase chain reaction (qRT-PCR). First, we verified the capability of NIR PT hyperthermia for cancer sensitization based on a significantly enhanced expression of the HSP gene family found in the NIR exposed group compared to the control (without NIR exposure) group after treating cancer cells with an identical concentration of Au@GO NPs (Figure 3g). Indeed, the upregulated HSP genes have been widely associated with reduced DNA repair in cancer cells and utilized for sensitizing cancer cells toward DNA-intercalating drugs such as doxorubicin.^[29,30] Therefore, Au@GO NPs could potentially lead to in vivo modulation of HSP genes in vivo by simply controlling laser intensities. Additionally, the Caspase 3 gene, a master cancer apoptotic gene, also dramatically increased (>fourfold) in the experimental Au@GO NP combined with NIR condition. Notably, unlike conventional PT-based anticancer therapies, our Au@GO NP-based mild PT hyperthermia effectively upregulated Caspase pathways without sacrificing cell viability (Figure S4, Supporting Information). However, when higher efficiency of cancer necrosis is needed, Au@GO NP can also induce cancer necrosis at over 90% efficiency by increasing laser intensity or nanoparticle concentration (Figure S4, Supporting Information). Considering the efficient PT induction of HSP and Caspase 3 at low laser intensities, Au@GO NP can effectively sensitize cancer cells toward gene and chemotherapies without potential phototoxicities (Figure S5, Supporting Information). Moreover, the spatiotemporally controlled gene regulation by PT hyperthermia can be desired for precise cancer therapy as well.

2.3. Sensitive Detection and Effective Suppression of Cancer Prosurvival Gene using Au@GO NP-NACs

The upregulated expression of the prosurvival BCL2 gene has been proven to be a cancer hallmark and suitable target for cancer diagnosis. As such, the unique physical properties (e.g., LSPR) and surface chemistry (e.g., reversible attachment and detachment of ASON) of Au@GO NP make it an excellent bifunctional platform for the monitoring and knockdown of BCL2 (Figure 4a).^[31,32,33] We demonstrated this by taking advantage of a reversible binding phenomenon between the GO and ASON interface. First, we loaded a Raman dye (Cy5)-labeled ASON (Cy5-ASON) onto Au@GO NP (Au@GO NP-Cy5-BCL2-NAC) based on the π - π interactions between ASON and graphene.^[10] When in the proximity of the Au NP core, the SERS

signal from the dye is strong, due to the LSPR effect. When the target complementary DNA or mRNA (e.g., BCL2 mRNA) is present in a double helix form, and the Cy5-ASON detaches from the surface of Au@GO NP. This leads to a Raman signal reduction (Figure 4a). Accompanying this process, the fluorescence of Cy5 is quenched in the proximity of Au@GO NP due to FRET and recovered when bound to the complementary DNA/mRNA sequence.^[19,26] Based on this mechanism, we first validated the detachment of the dye-conjugated ASON in the presence of complementary DNA/mRNA in a FRET assay (Figure 4b).

Next, we sought to investigate the possibility of mRNA detection via SERS by first using a solution-based assay followed by live-cell detection. From our results, as hypothesized, we found that when the dye-conjugated ASON was loaded onto the Au@GO NP, as characterized by X-ray photoelectron spectroscopy, multiple distinctive Cy5 Raman peaks appeared (Figure 4c; and Figure S6, Supporting Information). As soon as we incubated the Au@GO NP-ASON conjugates with complementary DNA sequences in a buffered solution, all characteristic peaks (e.g., 1120 cm⁻¹, aliphatic C-C vibration mode) of Cy5 diminished, suggesting the feasibility of SERS-based gene detection (Figure 4c). Meanwhile, considering the cellular uptake mechanism could vary among different cell types, we can also use an internal reference peak from GO (G band at 1650 cm⁻¹) to normalize different Au@GO NP-NACs uptake efficiency of various cells, thereby improving the reliability of the Au@GO NP-NAC-based sensing system.

Moreover, we demonstrated SERS-based nondestructive monitoring of cancer cells through a similar mechanism based on a reversible binding of ASON on the surface of Au@GO NP (Figure 4d,e). Specifically, transfecting a cancer cell known to express higher BCL2 mRNAs and a control noncancerous cell line with the Au@GO NP-Cy5-BCL2-NAC resulted in significantly different SERS spectrums. SERS peaks (1120 cm⁻¹) characteristics of the dye were 3–5 times lower in cancer cells compared to the control cells, suggesting a higher expression level of BCL2 (Figure 4d,e). Conventional gene analysis methods such as qRT-PCR validated the higher BCL2 mRNA expression in cancer cells with similar fold change, suggesting the potential of our Au@GO NP-NAC-based SERS platform for quantitative gene detection.^[33] However, quite interestingly, our approach does not require the lysis of cells for analysis, thereby providing live-cell detection. Additionally, since we used a NIR laser during SERS detection, our detection method could also be translated into in vivo systems. Therefore, by demonstrating the feasibility of Au@GO NP-NAC-based detection of cancer-related genes (BCL2 mRNAs) using nondestructive SERS methods, our Au@GO NP-NAC-based platform holds great promise in combined imaging and treatment of cancer cells.

Next, we confirmed the suppression of BCL2 mRNAs by Au@GO NP-NAC. Suppression of the overexpressed prosurvival BCL2 gene has been established as a promising treatment for cancer. However, many of BCL2 gene therapies have failed clinical trials, which can be partially attributed to the inconsistent therapeutic outcomes due to poor cellular uptake and enzymatic cleavage of genetic materials (e.g., ASON and siRNA).^[31,33,34] In this regard, both Au NP and

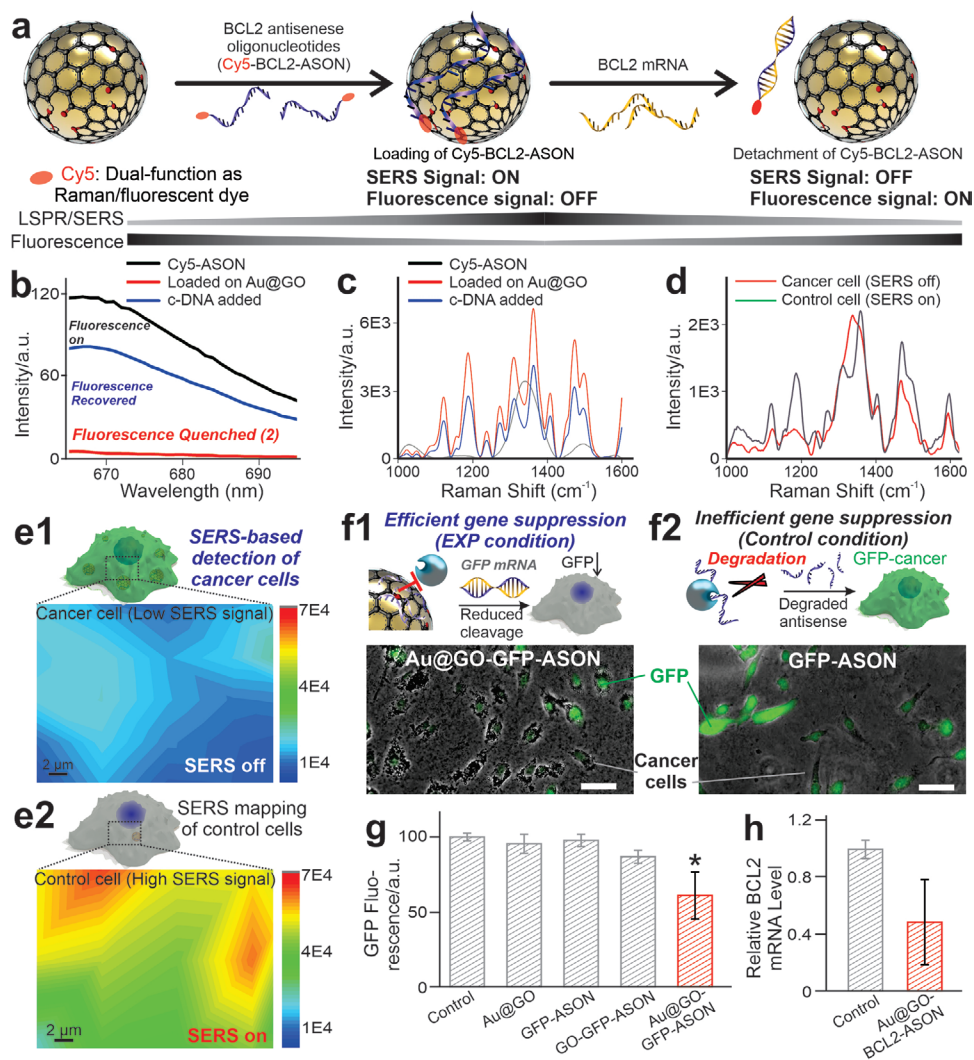


Figure 4. Au@GO NP-NACs for BCL2 gene suppression and live cancer cell detection. a) A schematic diagram showing the mechanism for gene sensing using Au@GO NP-NACs. b) Fluorescence quenching of a Cy5 labeled single-strand DNA during the adsorption onto Au@GO NP, and the fluorescence recovery after the antisense strand binds to the complementary DNA. The strong fluorescence at 670 nm wavelength from Cy5 labeled single-strand DNA [ssDNA-Cy5, gray line] was quenched immediately after the addition of Au@GO NP (red line) due to the FRET interaction between Cy5 and GO, and after adding complementary single-strand DNA (blue line), the ssDNA-Cy5 detached from the Au@GO NP and around 75% fluorescence was recovered. c,d) SERS spectra of in solution c) and in vitro d) cellular detection of target complementary DNA (c-DNA, c) or BCL2 mRNA overexpressed in cancer cells d). e) SERS mapping of cancer e1) and control e2) cells. The higher level of BCL2 mRNA expression in cancer cells results in the detachment of Raman-dye conjugated DNA probe and loss of SERS signals. f) A schematic diagram and fluorescent microscopy images representing the enhanced delivery of the GFP-ASON on the Au@GO NP delivery platform and the GFP knockdown in the U87-EGFP cell line. Scale bars: 100 μm. g) Summarized graphs showing the reduced green fluorescence in the GFP-labeled cancer cell line induced by Au@GO NP-GFP-ASON conjugates. h) Efficient BCL2 knockdown by Au@GO NP-BCL2-NAC. $n = 3$ biological replicates. * $P < 0.05$ by one-way ANOVA with Tukey post-hoc analysis.

GO have shown the potential to prevent enzymatic cleavage of antisense or siRNAs. Here, our Au@GO NP, with excellent cell transfection efficiency, could provide a unique platform for ASON delivery (Figure 4f).^[19,35] We first tested the efficacy of Au@GO NP-NACs for gene regulation based on a GFP knockdown assay using EGFP-labeled cancer cells (Figure 4f,g). We specifically designed the 21mer ASON sequence to bind with EGFP mRNAs and then loaded them onto Au@GO NP (Au@GO NP-GFP-NAC). By quantifying GFP fluorescence levels 48 h after treatment, we found gene suppression (around 30%) in our experimental group

(Au@GO NP-GFP-NAC) compared to the nontreated control. Further, to show the capability for cancer treatment, we delivered Au@GO NP-BCL2-NAC into cancer cells and monitored the gene expression using qRT-PCR (Figure 4h). Consistent with the GFP knockdown assay, we reduced BCL2 mRNA by 40% in our experimental (Au@GO NP-BCL2-NAC) condition compared to the control (no treatment). Therefore, using protein and gene expression assays, we successfully validated the enhanced delivery of ASONs and the suppression of a pro-survival (*BCL2*) gene in cancer cells via gene expression and protein assays.

2.4. Multicancer Cell Line Validation of a Target-Specific Synergistic Therapeutic Platform

An ideal cancer theragnostic system would allow the detection of cancer cells, followed by the effective suppression of tumors.^[5,6,36] Considering that gene therapy usually only targets specific pathways, recent evidence has suggested combinatorial treatment can significantly facilitate cancer gene therapy.^[13,33] In this regard, recent reports from our group, as well as many others, have shown synergy between hyperthermia and BCL2 gene downregulation for sensitizing cancer cells toward chemotherapy.^[28,29,32,33] Our Au@GO NP-based theragnostic platform is unique, as it not only can provide hyperthermia, BCL2 suppression, and anticancer drug delivery in a spatiotemporally controlled manner, but also allows for imaging of cancer cells and monitoring of gene delivery (Figure 5). More specifically, our Au@GO NP was employed to deliver doxorubicin (Au@GO NP-DOX), a topoisomerase II inhibitor drug, in an effort to initiate apoptotic pathways. In response to the doxorubicin, DNA repair mechanisms and antiapoptotic mechanisms in cancer take action to prevent cell death.^[37] To this end, Au@GO NP inhibits this process through overcoming two cancer therapeutic resistance mechanisms by i) inducing NIR-based PT hyperthermia, which stimulates HSP and reduces DNA repair, and ii) inhibiting the overexpressed BCL2 gene and shifting cancer cells toward proapoptotic status.^[32,33] Therefore,

synergistic induction of cancer apoptosis can be realized in a single platform (Figure 5a,b).

First, we verified their synergistic therapeutic effects using a cell apoptosis assay (Figure 5c). Consistent with our previous results, the Au@GO NP-based NIR hyperthermia alone does not induce noticeable cell death, suggesting minimum toxicity from our controlled mild hyperthermia (Figure S5, Supporting Information). However, the NIR hyperthermia significantly increased the toxicity of doxorubicin, indicating a robust synergistic effect between anticancer drugs and mild hyperthermia. Similarly, the delivery of Au@GO NP-BCL2-NAC sensitized cancer cells toward doxorubicin in a concentration-dependent manner. However, most importantly, Au@GO NP-BCL2-NAC combined with NIR hyperthermia promoted a significantly higher percentage of cell death compared to the control groups of the ASON alone (Au@GO NP-BCL2-NAC-DOX, by around 31%) and NIR hyperthermia alone (Au@GO NP-DOX, by around 17%) at the DOX loading concentration of $10 \mu\text{g mL}^{-1}$. The result from our optimized condition may originate from the simultaneous suppression of prosurvival BCL2 mRNAs (by ASON delivery) and an increase of proapoptotic mRNAs (e.g., Caspase, by NIR hyperthermia), which simultaneously enhance the potency of the delivered anticancer drug (Figure 5a).

Moreover, considering the high potency of the Au@GO NP-based platform, target-specific delivery would be essential to

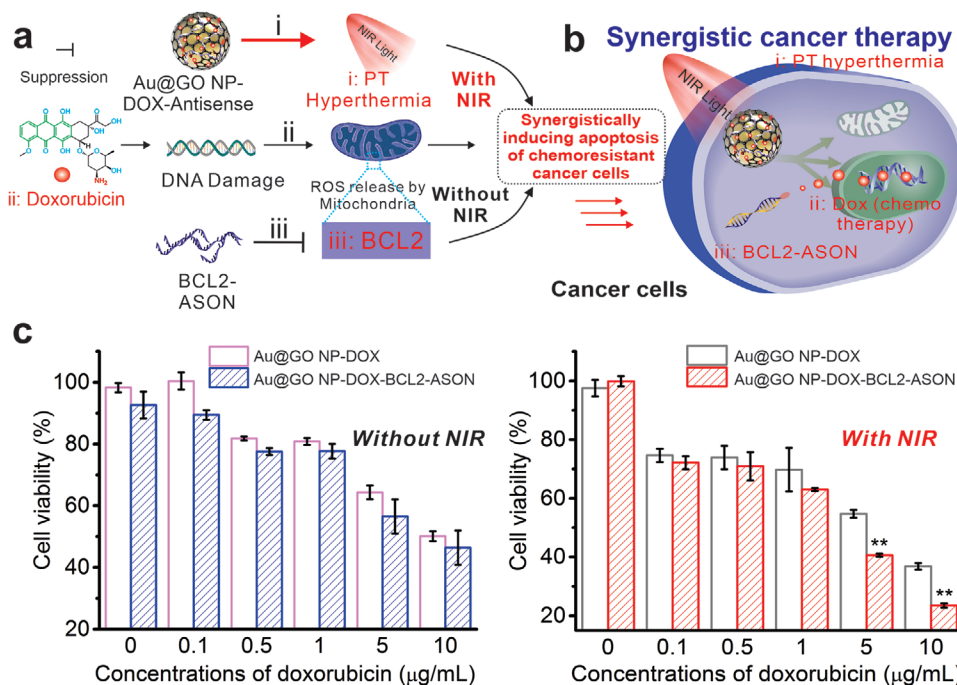


Figure 5. Synergistic cancer therapeutics based on Au@GO NP-NAC-enabled chemo/gene therapy and NIR PT hyperthermia. a) A schematic diagram depicting synergistic co-sensitization of cancer cells toward anticancer drug (DOX) through combined PT hyperthermia (NIR laser) treatment and BCL2-ASON delivery. b) The combined treatment mediated by Au@GO NP-NACs leads to synergistic cancer cell apoptosis. c) The cell viabilities of glioblastoma cells treated with the Au@GO NP carrying DOX only or both DOX and BCL2-ASON with or without NIR exposure. Without NIR irradiation (left), IC_{50} decreased from $10 \mu\text{g mL}^{-1}$ for Au@GO NP-DOX to around $6.7 \mu\text{g mL}^{-1}$ for Au@GO NP-DOX-BCL2-ASON. Through a further NIR irradiation, however, the IC_{50} of Au@GO NP-DOX-BCL2-ASON was decreased to $2.4 \mu\text{g mL}^{-1}$. On the other hand, NIR irradiation only (Au@GO NP-DOX on the right) decreased the IC_{50} of DOX from 10 to $5.4 \mu\text{g mL}^{-1}$. The apoptotic assay together with the aforementioned gene pathway studies supported the hypothesis in (a) that cancer cells can be synergistically sensitized toward chemotherapy by the combination of PT hyperthermia and BCL2-ASON in a single platform through a collective effect on the intracellular apoptotic pathways in cancer cells. $n = 3$ biological replicates. $**P < 0.01$ (compared to the control) by student's t -test.

avoid any side-effect on surrounding nontumor tissues. For this purpose, iRGD-conjugated lipid ligands were conjugated (iRGD-Au@GO NP) via hydrophobic interactions between a long carbon chain in the lipid and GO surfaces. Many cancer cells overexpress surface integrins, such as $\alpha\beta3$ that binds to iRGD, which has been established as a useful ligand for selective binding toward these integrins as well as enhancing tumor penetration in vivo.^[38] We confirmed the selective delivery of iRGD-Au@GO NP into $\alpha\beta3$ overexpressing malignant cells (MDA-MB-231) based on higher intracellular DFI signals comparing to a control cell line (MCF7) that does not overexpress the $\alpha\beta3$ integrin (Figure 6a1,a2). Most importantly, the selective delivery of the iRGD-Au@GO NP-BCL2-NAC-DOX combined with PT hyperthermia further resulted in an increased percentage of apoptotic malignant cells (Figure 6a3). Furthermore, not only for the breast cancer cells (MDA-MB-231), our iRGD-Au@GO-based therapeutic platform was further tested to be effective across nine different cancer cell lines with distinct

origins (liver, pancreas, lung, mammary gland, skin, and brain) in a combinatorial multicancer test (Figures S7 and S8, Supporting Information). Taken together, we established Au@GO NP-based synergistic cancer therapeutic platform for efficient and generalized cancer-killing without introducing significant toxicity in nontumor tissues, which are of utmost interest in clinical anticancer applications.

Additionally, we validated the effects of the Au@GO NP-based therapeutic platform for targeted cancer treatment in a microfluidic model. In the past few decades, many therapeutic strategies that killed cancer cells in vitro have failed in clinical trials due to heterogeneous cancer populations and complex tumor microenvironments in cancer patients.^[39] To this end, we evaluated the therapeutic potential of the iRGD-Au@GO NP-BCL2-NAC-DOX using a coculture microfluidic model (Figure 6b; and Figure S9, Supporting Information). More specifically, two pairs of cells of high clinical relevance are carefully selected to validate the therapeutic effects of our

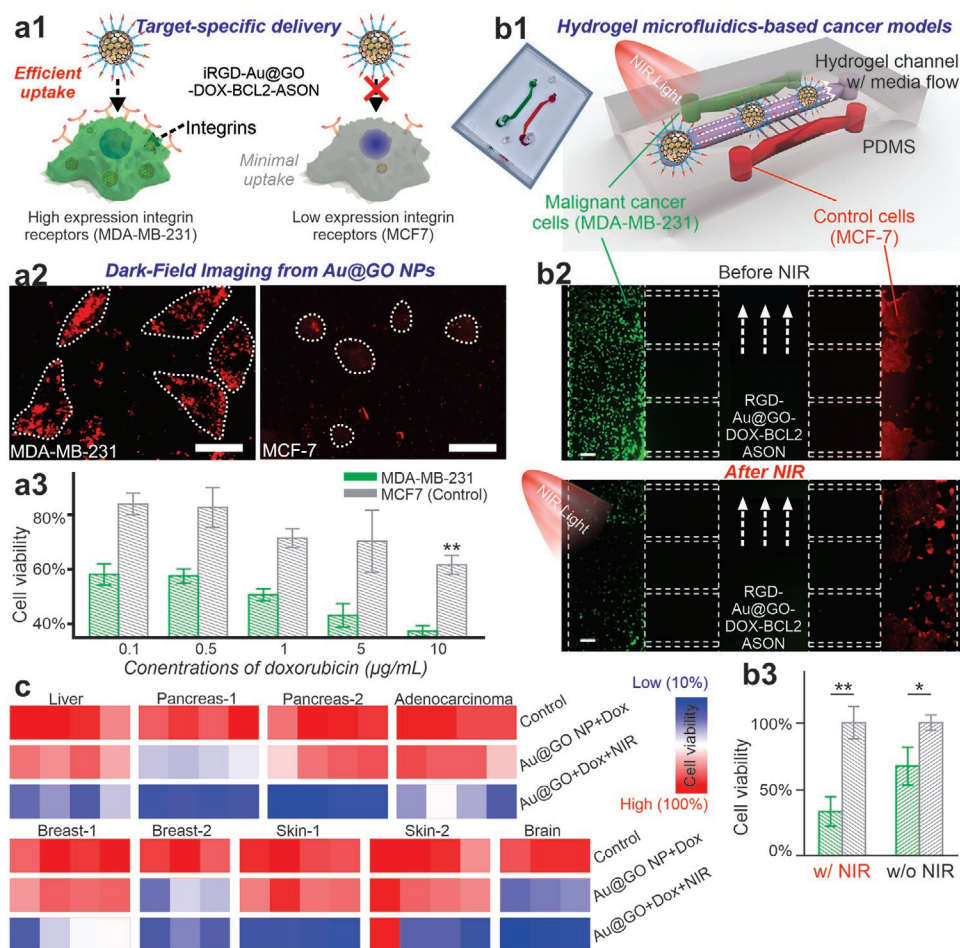


Figure 6. Targeted killing of cancer cells and the multicancer cell line validation of therapeutic effect of Au@GO NP-ASON platform. a) A schematic diagram a1) representing the functionalization of Au@GO NP with iRGD moieties (RGD-Au@GO NP) for the targeted delivery into cancer cells, and the corresponding DFI images (a2, scale bar: 100 μm) showing the selective uptake of iRGD-Au@GO NP by cells with high integrin (MDA-MB-231) compared to control cells (MCF7). As a result, the selective killing of high integrin-expression cancer cells (MDA-MB-231) was achieved a3). b) Schematic diagram b1), fluorescent microscope image b2), and quantifications b3) on the selective killing of targeted cells (GFP-MDA-MB-231, with RFP-MCF-7 as a control cell line) using a hydrogel-based microfluidic coculture model. In the center channel, Gel-MA hydrogels were placed to mimic the in vivo capillary vessels followed by the injection of iRGD-functionalized Au@GO NP particles. Error bars are standard deviation around the mean. $n = 3$ biological replicates. Scale bar: 100 μm . $*P < 0.05$, $**P < 0.01$ by student's t test. $n = 3$ independent experiments. c) Robust therapeutic effect of Au@GO NP-ASON platform validated in 9 cancer cell lines with distinctive tissue and organ origins.

platform: i) a control cell line (MCF-7) with low-integrin expression and a malignant/metastatic cancer cell line (MDA-MB-231) with high integrin expression, and ii) noncancerous astrocyte cell line and cancerous glioblastoma cell line. Compared to conventional in vitro cancer apoptosis assays, our microfluidic model may better represent the tumor microenvironment by providing: i) a center microchannel composed of photo-crosslinked gelatin-methacrylate hydrogels that mimic tumor vascularization; ii) a proper fluid flow rate that mimics the elution of nanoparticles and drugs in vivo; and iii) spatial patterning of heterogeneous cell populations that represent the heterogeneous structure of tumor tissues. Interestingly, we observed a robust migration of cancer cells through the microchannels 1 week after the establishment of the microfluidic model, indicating potential relevance to cancer invasion and metastasis (Figure 5b2; and Figure S9, Supporting Information). We mimicked intravenous and intratumoral injection of anticancer therapeutics by flowing drug-loaded Au@GO NP through the central channel and from the side channels, respectively. 2 days after nanoparticle treatment using an intravenous injection model followed by NIR treatment, we quantified cell apoptosis at each channel and found a higher (over 60%) reduction of cell viability and full ablation of migrating cells (MDA-MB-231) in the metastatic cancer cell channel (Figure 5b3). A similar trend was identified in the astrocyte-glioblastoma microfluidic model. In addition, the intratumoral injection model resulted in near 100% ablation of cancer cells (MCF7 and glioblastoma) without significantly reducing the survival of control cells (Figure S9, Supporting Information). These phenomena further confirmed the robust therapeutic effect from the Au@GO NP-based platform.

2.5. Au@GO NP-NACs for Advanced In Vivo Cancer Cell Imaging and Combined Therapeutics

With distinctive properties of Au@GO NP-NACs demonstrated in vitro, we then further performed an in vivo tumor growth assay to evaluate their theragnostic performance (Figure 7a). Considering the critical challenge of tumor heterogeneity, next-generation precision cancer medicine requires the treatment of cancer to start with detection, followed by the effective killing of cancer cells.^[40] While there have been quite a few nanoparticle-based NACs that effectively reduced tumor growth, there is still limited development of single-platform gene detection methods for probing cancer cells in vivo. In this regard, our Au@GO NP-NAC, which can target nucleic acids (e.g., BCL2 mRNA) in cancer and show significant changes in Raman signal, may provide a promising solution. To this end, we performed in vivo SERS on tumor and normal tissues 1 day post nanoparticle injection. Consistent with our in vitro experimental results as well as in vivo gene analysis, we found lower SERS signals at tumor sites compared to surrounding tissues, indicating a higher expression of BCL2 in vivo by cancer cells after the injection of Au@GO NP-Cy5-BCL2-NAC (Figure 7b,c). Similar trends were confirmed by Raman mapping as well (Figure 7b). While more detailed analysis would be required to evaluate the reliability of Au@GO NP-based SERS cancer gene detection, our results indicate the feasibility of Au@GO

NP-NACs for monitoring cancer cells in vivo. Next, we sought to investigate the anticancer therapeutic effects from the iRGD-Au@GO NP-BCL2-NAC-DOX. Consistent with our in vitro anticancer assays, our experimental group, which combines PT hyperthermia with gene and chemotherapies in a single platform, almost completely removed the tumor at the end of the in vivo assay (3 weeks) (Figure 7d,e). In contrast, all three control groups showed significantly lower tumor suppression, as quantified by the time-dependent tumor growth volumes. As such, we successfully validated the robust effect of our multifunctional Au@GO NP-based platform.

Additionally, gene analysis of the tumor tissues further revealed consistent mechanisms for cancer-killing, with a significant increase in the expression of apoptotic genes such as BID, BAX, Cyto-C, and Caspase 3 in our experimental group (Figure S10, Supporting Information). Also, no signs of toxicity from the conjugates were detected in normal tissues (Figure S10, Supporting Information). Taken together, we can conclude that the Au@GO NP-NAC-based treatment has an outstanding performance in tumor ablation with minimal toxic effects on noncancerous cells both in vitro and in vivo, which are all desired for precision cancer therapy. In parallel, as both GO and gold nanoparticles have been considered slow/nonbiodegradable, future studies would be essential to understand the in vivo metabolic and clearance pathways of our Au@GO NP-NACs before their clinical potential could be realized.^[41]

3. Conclusions

In the past two decades, nanoparticle-based NACs have shown great potential for theragnostic applications toward the treatment of cancer as well as many other diseases, but several limitations hindered their clinical applications. To this end, we developed a novel core-shell Au@GO NP-NACs with distinctive physical (e.g., NIR PT hyperthermia, DFI, SERS, and LSPR), chemical (e.g., reversible binding toward ASON) and biological properties (drug/gene delivery). As such, our Au@GO NP-NAC demonstrates a high contrast DFI modality enabling cancer imaging in vitro, as well as the selective detection of an over-expressed cancer gene achieved by SERS sensing. In addition, the suppression of a prosurvival gene, combined with phototherapy and chemotherapy mediated by Au@GO NP-NAC, led to the synergistic induction of cancer apoptosis. The establishment of a cancer coculture microfluidic model validated the target-specificity of Au@GO NP-NAC, and in vivo tumor growth assays supported its clinical promise of combinatorial treatment of cancer. While many nanoparticles and NACs have been studied for cancer theragnostics, our approach based on Au@GO NP-NACs allows the practical identification and robust killing of 9 different types of cancer cells with distinctive tissue origins in a single platform, which is desired for next-generation precision cancer therapy.

Nondestructive diagnosis and selective modulation of genes have been utilized to facilitate the development of many biomedical fields. Combining gene therapy with phototherapies (e.g., PT hyperthermia) has also shown promise for cancer treatment, regenerative medicine, and neurodegenerative diseases.^[5,40] For this purpose, our Au@GO NP-NAC, as a modular theragnostic platform, holds great potential for a variety of advanced applications.

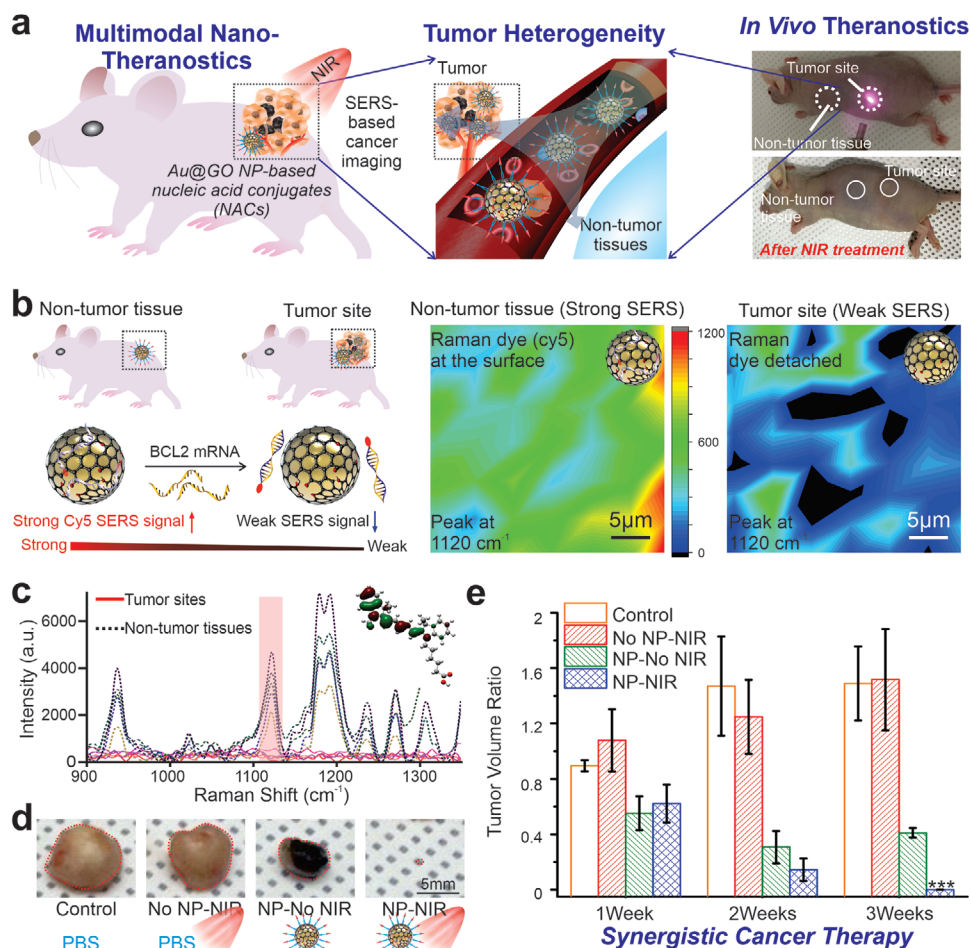


Figure 7. Au@GO NP-ASON conjugates for detection and efficient suppression of tumor in vivo. a) Schematic diagrams (in the left and middle panel) showing the Au@GO NP-based theranostic applications for in vivo cancer nanotheranostic applications. Images on the right: Photographs showing the process of photothermal treatment at the tumor sites and the detection of genes through SERS. b,c) A schematic diagram (left panel in (b)), SERS mapping results (Right panels in (b)) and representative in vivo SERS spectrum supporting the effective detection of cancer cells in vivo by observing a significant difference in the SERS signals at the tumor site and surrounding nontumor tissues. c) In vivo SERS (5 spectra per group) illustrating the distinctive differences between tumor sites and nontumor sites after injected with Au@GO NP-ASON conjugates. d) Representative photographs of tumor extracted from mice after 3 weeks of treatment under different conditions showing the robust anticancer effects in vivo of the Au@GO NP-NAC-based combined therapeutics. e) Time-dependent change of tumor volume under different treatment under different conditions. This result shows the significant tumor suppression by Au@GO NP-ASON conjugates loaded with DOX and irradiated by NIR laser, leading to a near-complete ablation of tumors. $***P < 0.01$ by one-way ANOVA with Tukey post-hoc analysis. $n = 3$ independent experiments.

For example, the detection and silencing of miRNAs that regulate cancer metastasis can lead to new devices that facilitate cancer therapies. Similarly, both photothermal treatment and nanoparticle-mediated siRNA delivery have been considered promising approaches for modulating tumor microenvironments. Also, further enhancement of the distinctive physical properties of Au@GO NP-NAC, such as the LSPR, could improve its overall therapeutic effects. These could be achieved by modulating the shape and components of the plasmonic core nanoparticles. Additionally, developing biodegradable or biocleavable versions of Au@GO NP by controlling its composition may also speed up its clinical translation significantly. Moving forward, we expect to establish quantitative and multiplex gene detection for a better understanding of complex diseases.

Taken together, the successful further development of multifunctional Au@GO NP-NAC-based nanotheranostic platform

would pave new roads for next-generation precision medicine, not only for the treatment of but also to accurately diagnose and effectively prognose cancer and other diseases that are complicated by a multitude of genetic/epigenetic alternations.

Supporting Information

Supporting Information is available from the Wiley Online Library or from the author.

Acknowledgements

This work was partially supported by NSF (No. CHE-1429062, CBET-1803517), the New Jersey Commission on Spinal Cord Research (Nos. CSCR17IRG010 and CSCR16ERG019), NIH R21 (No. R21AR071101),

and NIH R01 (Nos. 1R01DC016612, 3R01DC016612-01S1, and 5R01DC016612-02S1). All animals were acclimatized to the animal facility for at least 48 hours before experimentation and maintained according to the Guide for the Care and Use of Laboratory Animals published by the NIH. The animal protocol was approved by the Institutional review board of the Korea University (protocol number:1040548-KU-IRB-13-9-A-1).

Conflict of Interest

The authors declare no conflict of interest.

Keywords

graphene hybrid nanomaterials, multimodal cancer theragnostics, nanomedicine, nanoparticle-based nucleic acid conjugates, personalized medicine

Received: August 15, 2020

Revised: October 6, 2020

Published online:

- [1] a) M. Vishwakarma, E. Piddini, *Nat. Rev. Cancer* **2020**, *20*, 187; b) J. Hausser, U. Alon, *Nat. Rev. Cancer* **2020**, *20*, 247.
- [2] a) H. W. Jackson, J. R. Fischer, V. R. T. Zanotelli, H. R. Ali, R. Mechera, S. D. Soysal, H. Moch, S. Muenst, Z. Varga, W. P. Weber, B. Bodenmiller, *Nature* **2020**, *578*, 615; b) N. S. Fox, S. Haider, A. L. Harris, P. C. Boutros, *Nat. Commun.* **2019**, *10*, 13; c) Z. H. Miao, D. D. Huang, Y. C. Wang, W. J. Li, L. N. Fan, J. G. Wang, Y. Ma, Q. L. Zhao, Z. B. Zha, *Adv. Funct. Mater.* **2020**, *30*, 2001593; d) Y. B. Wang, W. B. Wu, D. Mao, C. Teh, B. Wang, B. Liu, *Adv. Funct. Mater.* **2020**, *30*, 11.
- [3] Á. Quintanal-Villalonga, J. M. Chan, A. Y. Helena, D. Pe'er, C. L. Sawyers, S. Triparna, C. M. Rudin, *Nat. Rev. Clin. Oncol.* **2020**, *17*, 360.
- [4] a) Q. Jin, Y. Y. Deng, X. H. Chen, J. Ji, A. C. S. Nano, **2019**, *13*, 954; b) J. Mu, J. Lin, P. Huang, X. Chen, *Chem. Soc. Rev.* **2018**, *47*, 5554.
- [5] J. Shi, P. W. Kantoff, R. Wooster, O. C. Farokhzad, *Nat. Rev. Cancer* **2017**, *17*, 20.
- [6] W. C. Chan, A. Khademhosseini, W. Parak, P. S. Weiss, *ACS Nano* **2017**, *11*, 4375.
- [7] a) D.-E. Lee, H. Koo, I.-C. Sun, J. H. Ryu, K. Kim, I. C. Kwon, *Chem. Soc. Rev.* **2012**, *41*, 2656; b) Y. Sun, Y. J. Wang, C. C. Niu, E. M. Strohm, Y. Y. Zheng, H. T. Ran, R. Z. Huang, D. Zhou, Y. P. Gong, Z. G. Wang, D. Wang, M. C. Kolios, *Adv. Funct. Mater.* **2020**, *30*, 1.
- [8] a) A. Kundu, S. Nandi, A. K. Nandi, *Prog. Mater. Sci.* **2017**, *88*, 136; b) E. P. Thi, C. E. Mire, A. C. H. Lee, J. B. Geisbert, J. Z. Zhou, K. N. Agans, N. M. Snead, D. J. Deer, T. R. Barnard, K. A. Fenton, I. MacLachlan, T. W. Geisbert, *Nature* **2015**, *521*, 362.
- [9] a) J. I. Cutler, E. Auyeung, C. A. Mirkin, *J. Am. Chem. Soc.* **2012**, *134*, 1376; b) H. Rabie, Y. X. Zhang, N. Pasquale, M. J. Lagos, P. E. Batson, K. B. Lee, *Adv. Mater.* **2019**, *31*, 8.
- [10] L. Yang, J.-H. Lee, C. Rathnam, Y. Hou, J.-W. Choi, K.-B. Lee, *Nano Lett.* **2019**, *19*, 8138.
- [11] E. Zeggini, A. L. Gloyn, A. C. Barton, L. V. Wain, *Science* **2019**, *365*, 1409.
- [12] L. H. Tang, H. X. Chang, Y. Liu, J. H. Li, *Adv. Funct. Mater.* **2012**, *22*, 3083.
- [13] C. Chakraborty, A. R. Sharma, G. Sharma, C. G. P. Doss, S.-S. Lee, *Mol. Ther.– Nucleic Acids* **2017**, *8*, 132.
- [14] G. Chen, Y. Wang, R. Xie, S. Gong, *J. Controlled Release* **2017**, *259*, 105.
- [15] N. Panwar, A. M. Soehartono, K. K. Chan, S. W. Zeng, G. X. Xu, J. L. Qu, P. Coquet, K. T. Yong, X. Y. Chen, *Chem. Rev.* **2019**, *119*, 9559.
- [16] V. Giannini, A. I. Fernandez-Dominguez, S. C. Heck, S. A. Maier, *Chem. Rev.* **2011**, *111*, 3888.
- [17] P. T. Yin, S. Shah, M. Chhowalla, K. B. Lee, *Chem. Rev.* **2015**, *115*, 2483.
- [18] a) K. Yang, L. Feng, X. Shi, Z. Liu, C. S. Rev, **2013**, *42*, 530; b) A. Paul, A. Hasan, H. Al Kindi, A. K. Gaharwar, V. T. S. Rao, M. Nikkhah, S. R. Shin, D. Krafft, M. R. Dokmeci, D. Shum-Tim, A. Khademhosseini, *ACS Nano* **2014**, *8*, 8050; c) A. H. Hung, R. J. Holbrook, M. W. Rotz, C. J. Glasscock, N. D. Mansukhani, K. W. MacRenaris, L. M. Manus, M. C. Duch, K. T. Dam, M. C. Hersam, T. J. Meade, *ACS Nano* **2014**, *8*, 10168; d) Z. X. Tu, E. G. Donskyi, H. S. Qiao, Z. L. Zhu, W. E. S. Unger, C. P. R. Hackenberger, W. Chen, M. Adeli, R. Haag, *Adv. Funct. Mater.* **2017**, *27*, 1701837.
- [19] L. H. Tang, Y. Wang, J. H. Li, *Chem. Soc. Rev.* **2015**, *44*, 6954.
- [20] S. Laing, L. E. Jamieson, K. Faulds, D. Graham, *Nat. Rev. Chem.* **2017**, *1*, 0060.
- [21] a) S. Mao, G. H. Lu, K. H. Yu, Z. Bo, J. H. Chen, *Adv. Mater.* **2010**, *22*, 3521; b) J. H. Lee, H. K. Choi, L. Yang, S. T. D. Chueng, J. W. Choi, K. B. Lee, *Adv. Mater.* **2018**, *30*, 8; c) A. Doerr, *Nat. Methods* **2019**, *16*, 578; d) L. Xiong, C. Forsythe, M. Jung, A. S. McLeod, S. S. Sunku, Y. M. Shao, G. X. Ni, A. J. Sternbach, S. Liu, J. H. Edgar, E. J. Mele, M. M. Fogler, G. Shvets, C. R. Dean, D. N. Basov, *Nat. Commun.* **2019**, *10*, 6; e) H. J. Yin, H. J. Tang, D. Wang, Y. Gao, Z. Y. Tang, *ACS Nano* **2012**, *6*, 8288.
- [22] D. K. Lim, A. Barhoumi, R. G. Wylie, G. Reznor, R. S. Langer, D. S. Kohane, *Nano Lett.* **2013**, *13*, 4075.
- [23] A. Albanese, P. S. Tang, W. C. Chan, *Annu. Rev. Biomed. Eng.* **2012**, *14*, 1.
- [24] B. D. Chithrani, A. A. Ghazani, W. C. Chan, *Nano Lett.* **2006**, *6*, 662.
- [25] X. Huang, S. Neretina, M. A. El-Sayed, *Adv. Mater.* **2009**, *21*, 4880.
- [26] C. H. Lu, H. H. Yang, C. L. Zhu, X. Chen, G. N. Chen, *Angew. Chem., Int. Ed.* **2009**, *48*, 4785.
- [27] C. Zhang, Y. Yuan, S. Zhang, Y. Wang, Z. Liu, *Angew. Chem., Int. Ed.* **2011**, *50*, 6851.
- [28] R. Setroikromo, P. Wierenga, M. Van Waarde, J. Brunsting, E. Vellenga, H. Kampinga, *Cell Stress Chaperones* **2007**, *12*, 320.
- [29] P. T. Yin, B. P. Shah, K. B. Lee, *Small* **2014**, *10*, 4106.
- [30] P. Wust, B. Hildebrandt, G. Sreenivasa, B. Rau, J. Gellermann, H. Riess, R. Felix, P. M. Schlag, *Lancet Oncol.* **2002**, *3*, 487.
- [31] W. T. Sun, X. Y. Chen, C. Xie, Y. Wang, L. T. Lin, K. S. Zhu, X. T. Shuai, *Biomacromolecules* **2018**, *19*, 2248.
- [32] a) H. Thomadaki, A. Scorilas, *Crit. Rev. Clin. Lab. Sci.* **2006**, *43*, 1; b) A. M. Chen, M. Zhang, D. G. Wei, D. Stueber, O. Taratula, T. Minko, H. X. He, *Small* **2009**, *5*, 2673.
- [33] B. Jansen, V. Wacheck, E. Heere-Ress, H. Schlagbauer-Wadl, C. Hoeller, T. Lucas, M. Hoermann, U. Hollenstein, K. Wolff, H. Pehamberger, *Lancet* **2000**, *356*, 1728.
- [34] A. Frenzel, F. Grespi, W. Chmielewski, A. Villunger, *Apoptosis* **2009**, *14*, 584.
- [35] a) W. Pan, B. Liu, X. Gao, Z. Yu, X. Liu, N. Li, B. Tang, *Nanoscale* **2018**, *10*, 14264; b) C.-H. Lu, C.-L. Zhu, J. Li, J.-J. Liu, X. Chen, H.-H. Yang, *Chem. Commun.* **2010**, *46*, 3116; c) L.-S. Lin, Z.-X. Cong, J.-B. Cao, K.-M. Ke, Q.-L. Peng, J. Gao, H.-H. Yang, G. Liu, X. Chen, *ACS Nano* **2014**, *8*, 3876.
- [36] C. Chen, S. Zhou, Y. Cai, F. Tang, *npj Precis. Oncol.* **2017**, *1*, 37.
- [37] L. N. Abdullah, E. K.-H. Chow, *Clin. Transl. Med.* **2013**, *2*, 3.
- [38] K. N. Sugahara, T. Teesalu, P. P. Karmali, V. R. Kotamraju, L. Agemy, D. R. Greenwald, E. Ruoslahti, *Science* **2010**, *328*, 1031.
- [39] K. E. Sung, D. J. Beebe, *Adv. Drug Delivery Rev.* **2014**, *79-80*, 68.
- [40] a) M. Li, X. Yang, J. Ren, K. Qu, X. Qu, *Adv. Mater.* **2012**, *24*, 1722; b) A. Donde, P. C. Wong, L. L. Chen, *Curr. Gene Ther.* **2017**, *17*, 187; c) R. A. Smith, T. M. Miller, K. Yamanaka, B. P. Monia, T. P. Condon, G. Hung, C. S. Lobsiger, C. M. Ward, M. McAlonis-Downes, H. Wei, *J. Clin. Invest.* **2006**, *116*, 2290; d) M. Srikanth, J. A. Kessler, *Nat. Rev. Neurol.* **2012**, *8*, 307.
- [41] B. Wang, X. He, Z. Zhang, Y. Zhao, W. Feng, *Acc. Chem. Res.* **2013**, *46*, 761.